Robust Tracking of Bio-Inspired References for a Biped Robot Using Geometric Algebra and Sliding Mode Control

J. Oviedo-Barriga, L. González-Jiménez,
B. Castillo-Toledo and E. Bayro-Corrochano

Abstract. Controlling walking biped robots is a challenging problem due to its complex and uncertain dynamics. In order to tackle this, we propose a sliding mode controller based on a dynamic model which was obtained using the conformal geometric algebra approach (CGA). The CGA framework permits us to use lines, points, and other geometric entities, to obtain the Lagrange equations of the system. The references for the joints of the robot were bio-inspired in the kinematics of a walking human body. The first and second derivatives of the reference signal were obtained through an exact robust differentiator based on high order sliding mode. The performance of the proposed control schemes are illustrated through simulation.

Keywords. Bio-inspired signal, tracking, conformal geometric algebra.

1. Introduction

The control of bipedal walking robot is a complex task due to several degrees of freedom, highly nonlinear dynamics, and a complicated model to describe the behavior of the walking robot. For this reason, we analyze each leg of the biped robot as a serial robotic system and synthesize the dynamic model via the Lagrange equations using the conformal geometric (CGA) approach. The CGA approach allows us to obtain, through a simple procedure, a compact representation of the dynamics of a robotic mechanism. This is due to the simple representation of rigid transformations (rotations, translations, screw motions and others) and geometric entities (points, lines, planes, circles, spheres, point pairs, etc) in this framework [1].

This work was supported in part by PhD scholarships no. 28824.

The references for each joint of the biped robot were obtained using the Humanoid Robots Simulation Platform (HRSP) [2], a Simulink Toolbox developed by the group of Aleksandar Rodic [3].

In addition, a first and second order sliding mode controllers were designed to perform tracking of the bio-inspired references for the biped robot. Sliding mode control is widely used in uncertain or disturbed systems, featuring robustness and accuracy [4]. An important drawback of the standard sliding mode controller is the presence of high frequency components in the control signals due to the switching function used in its design. In order to attenuate this effect we use sigmoid functions in the proposed controller and we also use *super twisting* technique as another solution to reduce the high frequencies [10, 11].

The document is organized as follows. Section II presents a brief introduction to the Conformal Geometric Algebra. The dynamic model for the pose of robotic manipulators is obtained in Section III. The design of the error variables and sliding mode controllers in CGA are presented in Section IV. Also, the structure for the exact robust differentiator is explained. In section V shows a simulation of the application of the designed controllers in a 12 DOF biped robot. Finally, conclusions are given in Section VI.

2. Conformal Geometric Algebra

The Euclidean vector space $\mathbb{R}^3$ can be represented in geometric algebra $G_{4,1}$ and treat conformal geometry in an advantageous manner [1]. This algebra has an orthonormal vector basis given by $\{e_i\}$ and a bivectorial basis defined as $e_{ij} = e_i \wedge e_j$, $e_i \wedge e_\infty$ for $i, j = \{0, 1, 2, 3\}$.

The bivectors e_{23}, e_{31} y e_{12} correspond to the Hamilton basis and $E = e_\infty \wedge e_0$ is the Minkowsky plane. The unit Euclidean pseudo-scalar $I := e_1 \wedge e_2 \wedge e_3$, the conformal pseudoscalar $I_c = I_e E$ is used for computing the inverse and duals of multivectors. For more about conformal geometric algebra, see [1, 5].

Let $x_e = [x, y, z]^T$ be a point expressed in $\mathbb{R}^3$. The representation of this point in the geometric algebra $G_{4,1}$ is given by

$$x_c \quad = \quad x_e + \frac{1}{2} x_e^2 e_\infty + e_0, \tag{2.1}$$

where the null vectors are the point at infinity e_∞ and the origin point e_0, with the properties $e_\infty^2 = e_0^2 = 0$ and $e_\infty \cdot e_0 = 1$.

Given two conformal points x_c and y_c, its difference in Euclidean space can be defined as

$$x_e - y_e = (y_c \wedge x_c) \cdot e_\infty, \tag{2.2}$$

and, consequently, the following equality:

$$(x_c \wedge y_c + y_c \wedge z_c) \cdot e_\infty = (x_c \wedge z_c) \cdot e_\infty \tag{2.3}$$

is fulfilled as well.

The line can be obtained in its standard form as

$$L = \mathbf{n} I_e - e_\infty \mathbf{m} I_e, \tag{2.4}$$

where $\mathbf{n}$ is the orientation and $\mathbf{m}$ the moment of the line.

3. Rigid transformations

These transformations between rigid bodies can be obtained in conformal geometry by carrying out reflections between planes.

3.1. Reflection

A reflection of a point x respect to a plane π is

$$x' = -\pi x \pi^{-1}, \tag{3.1}$$

and for any geometric entity Q is

$$Q' = -\pi Q \pi^{-1}, \tag{3.2}$$

3.2. Traslation

The translation can be carrying out by two reflections with parallel planes π_1 and π_2 as

$$Q' = \underbrace{(\pi_2 \pi_1)}_{T_a} Q \underbrace{(\pi_1^{-1} \pi_2^{-1})}_{\tilde{T}_a}, \quad T_a = 1 + \tfrac{1}{2} a e_\infty = e^{-\frac{a}{2} e_\infty}, \tag{3.3}$$

with $a = 2dn$, d the distance of translation and n the direction of translation.

3.3. Rotation

A rotation is the product of two reflections between nonparallel planes π_1 and π_2 cross the origin. The rotation is then defined by

$$Q' = \underbrace{(\pi_2 \pi_1)}_{R_\theta} Q \underbrace{(\pi_1^{-1} \pi_2^{-1})}_{\tilde{R}_\theta}. \tag{3.4}$$

Computing the conformal product of the normal of the planes n_1 and n_2, yields

$$R_\theta = n_2 n_1 = \cos(\theta/2) - \sin(\theta/2)\, L = e^{-\theta L/2}, \tag{3.5}$$

with $L = n_1 \wedge n_2$, and θ twice the angle between π_1 and π_2.

3.4. Screw motion

The screw motion called motor is a composition of a translation and a rotation, both related to an arbitrary axis L. The motor is defined as

$$M = TR\tilde{T}. \tag{3.6}$$

Therefore, a motor transformation for an entity Q is given by

$$Q' = \underbrace{\left(TR\tilde{T}\right)}_{M_\theta} Q \underbrace{\left(T\tilde{R}\tilde{T}\right)}_{\tilde{M}_\theta}. \tag{3.7}$$

A more detailed description of Conformal Geometric Algebra can be found in [1] and [5].

4. Dynamic modelling using CGA

Based on the equations of kinetic and potential energy and using the Euler Lagrange formulation, it is possible to synthesize the dynamic model of any n-DOF serial robot manipulator in terms of CGA [7]. The matrix form of the Euler Lagrange equation is given by

$$M(q)\,\ddot{q} + C(q,\dot{q})\,\dot{q} + G(q) = \tau. \tag{4.1}$$

Defining m_i, I_j, L_i' and x_i'as the mass, moment of inertia, current axis of rotation and current position of the center of mass for the i^{th} link of the manipulator respectively, it is possible to re-define equation (4.1) in the CGA framework using the following matrices

$$M(q) = M_v + M_I, \tag{4.2}$$

where

$$M_I = \delta I = \begin{pmatrix} 1 & 1 & \cdots & 1 \\ 0 & 1 & \cdots & 1 \\ \vdots & \vdots & \ddots & \vdots \\ 0 & 0 & \cdots & 0 \end{pmatrix} \begin{pmatrix} I_1 & 0 & \cdots & 0 \\ I_2 & I_2 & \cdots & 0 \\ \vdots & \vdots & \ddots & \vdots \\ I_n & I_n & \cdots & I_n \end{pmatrix}, \tag{4.3}$$

and

$$M_v = V^T m V, \tag{4.4}$$

whit $m = diag\{m_1, m_2, \cdots, m_n\}$ and

$$V = \begin{pmatrix} x_1' \cdot L_1' & 0 & \cdots & 0 \\ x_2' \cdot L_1' & x_2' \cdot L_2' & \cdots & 0 \\ \vdots & \vdots & \ddots & \vdots \\ x_n' \cdot L_1' & x_n' \cdot L_2' & \cdots & x_n' \cdot L_n' \end{pmatrix}. \tag{4.5}$$

Based in the properties of the matrices $M(q)$, $C(q,\dot{q})$ as

$$C = V^T m \dot{V}, \tag{4.6}$$

where

$$V = XL = \begin{pmatrix} x_1' & 0 & \cdots & 0 \\ 0 & x_2' & \cdots & 0 \\ \vdots & \vdots & \ddots & \vdots \\ 0 & 0 & \cdots & x_n' \end{pmatrix} \begin{pmatrix} L_1' & 0 & \cdots & 0 \\ L_1' & L_2' & \cdots & 0 \\ \vdots & \vdots & \ddots & \vdots \\ L_1' & L_2' & \cdots & L_n' \end{pmatrix}. \tag{4.7}$$

Therefore,

$$\dot{V} = \dot{X}L + X\dot{L}, \tag{4.8}$$

where

$$\dot{X} = \begin{pmatrix} \dot{x}_1' & 0 & \cdots & 0 \\ 0 & \dot{x}_2' & \cdots & 0 \\ \vdots & \vdots & \ddots & \vdots \\ 0 & 0 & \cdots & \dot{x}_n' \end{pmatrix}, \qquad \dot{L} = \begin{pmatrix} \dot{L}_1' & 0 & \cdots & 0 \\ 0 & \dot{L}_2' & \cdots & 0 \\ \vdots & \vdots & \ddots & \vdots \\ 0 & 0 & \cdots & \dot{L}_n' \end{pmatrix}. \tag{4.9}$$

Finally, the vector $G(q)$ is expressed as the following product

$$G(q) = V^T F, \tag{4.10}$$

with

$$F = \begin{pmatrix} m_1 & 0 & \cdots & 0 \\ 0 & m_2 & \cdots & 0 \\ \vdots & \vdots & \ddots & \vdots \\ 0 & 0 & \cdots & m_n \end{pmatrix} \begin{pmatrix} ge_2 \\ ge_2 \\ ge_2 \\ ge_2 \end{pmatrix}, \tag{4.11}$$

where g is the acceleration due to gravity. Thus equation (4.1) will be rewritten as

$$\delta I \ddot{q} + V^T m(V\ddot{q} + \dot{V}\dot{q} + a) = \tau, \tag{4.12}$$

Note that by means the equation (4.12) the terms are obtained using just inner products between X_i' and L_i'. For a more detailed explanation of the process to obtain (4.1) see [7]. By mean equation (4.12) and using measurements of the X_i' and L_i', we can compute the involved tensor of (4.1). In our simulation we compute these tensor step by step in this way, (see Figure 1).

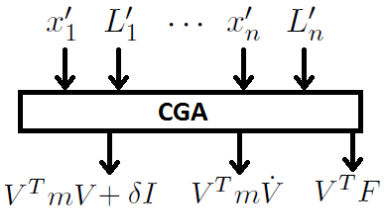

FIGURE 1. Measurements for tensors.

5. Sliding mode controller

In this section, the output tracking problem will be developed for the two legs in the biped robot, each with 6-DOF, and a sliding mode controller will be proposed [8, 12]. Due to space limitation the procedure will be explained only for the left leg. Adding a disturbance term $P(t)$ to (4.1), we can obtain a state-space representation defining the state variables as $x_1 = q$, $x_2 = \dot{q}$, the output of the system as $y = x_1$ and the control signal as $U = \tau$. Hence, the resulting state-space model is given by

$$\begin{aligned} \dot{x}_1 &= x_2, \\ \dot{x}_2 &= -M^{-1}\left(Cx_2 + G\right) + M^{-1}U + P(t), \end{aligned} \tag{5.1}$$

the parenthesis were omitted for simplicity and the entries of the tensor were computed using equation (4.12). We assume that the disturbance term $P(t)$ is bounded as follows

$$\|P\left(t\right)\| < \beta. \tag{5.2}$$

5.1. Fist order sliding mode control

Defining the output tracking error as

$$e_1 = x_1 - y_{ref}\left(t\right). \tag{5.3}$$

where y_{ref} is the bio-inspired references for the biped robot mentioned in a previous section. Then, the dynamic for e_1 is given by

$$\dot{e}_1 = x_2 - \dot{y}_{ref}\left(t\right). \tag{5.4}$$

Using x_2 as the pseudo-control for this block, we obtain its reference x_2ref as

$$x_{2ref} = -k_1 \tanh\left(\varepsilon_1 e_1\right) + \dot{y}_{ref}\left(t\right). \tag{5.5}$$

Then, if we define the error variable for the second block as

$$e_2 = x_2 - x_{2ref}, \tag{5.6}$$

its dynamics can be obtained as

$$\dot{e}_2 = -M^{-1}\left(Cx_2 + G\right) + M^{-1}U + P\left(t\right) - \dot{x}_{2ref}. \tag{5.7}$$

The term $\dot{x}_{2ref}$ is defined as

$$\dot{x}_{2ref} = -k_1\varepsilon_1\Phi\left(x_2 - \dot{y}_{ref}\left(t\right)\right) + \ddot{y}_{ref}\left(t\right) \tag{5.8}$$

with $\Phi = diag\left\{\ 1-\tanh^2\left(\varepsilon_1 e_{11}\right),\quad \cdots,\quad 1-\tanh^2\left(\varepsilon_1 e_{1n}\right)\ \right\}$ and $e_1 = \left[\ e_{11}\quad \cdots\quad e_{1n}\ \right]^T$.

Finally, we design the control law U as

$$U = Cx_2 + G - k_2 M\ sign\left(\varepsilon_2 e_2\right) + M\dot{x}_{2ref}. \tag{5.9}$$

By means of (5.9), (5.7), (5.5), and (5.4) the closed loop dynamics for the error variables is given by

$$\begin{aligned} \dot{e}_1 &= -k_1 \tanh\left(\varepsilon_1 e_1\right), \\ \dot{e}_2 &= -k_2\ sign\left(\varepsilon_2 e_2\right) + P\left(t\right). \end{aligned} \tag{5.10}$$

If the conditions $k_1 > 0$, $k_2 > \beta$ are fulfilled, then the system (5.10) is globally asymptotically stable [8].

A model of the robot humanoid is presented in Figure 2. It is a 3-D virtual representation of the Mexone humanoid robot from CINVESTAV, Campus Guadalajara. Each leg of the biped robot has 6 DOF: 3 in the hip, 1 in the knee, and 2 in the ankle.

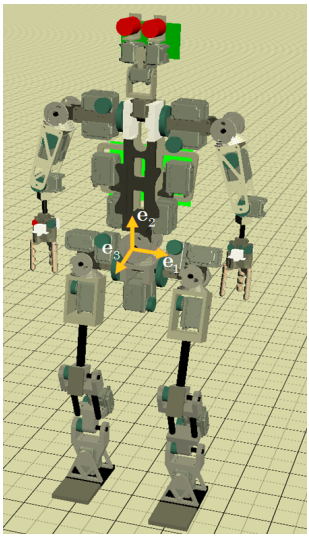

FIGURE 2. Biped robot with 6-DOF per leg.

5.2. Second order sliding mode control

One of advantages of second order sliding mode control is that it reduces high frequency components in the control signal. This technique is known as *Super Twisting* [10, 11].

Starting of state-space model (5.1) the tracking error e_1 is defined as

$$e_1 = x_1 - y_{ref}. \tag{5.11}$$

Then, the dynamic for e_1 is given by

$$\dot{e}_1 = x_2 - \dot{y}_{ref} = -k_1 e_1. \tag{5.12}$$

Using x_2 as the pseudo-control for this block, the reference x_{2ref} is obtained as

$$x_{2ref} = \dot{y}_{ref} - k_1 e_1. \tag{5.13}$$

Then, the error variable for the second block is defined as

$$e_2 = x_2 - x_{2ref}, \tag{5.14}$$

its dynamics can be obtained as

$$\dot{e}_2 = -M^{-1}\left(Cx_2 + G\right) + M^{-1}\tau + P(t) - \dot{x}_{2ref}, \tag{5.15}$$

where the control law is proposed as

$$\tau = \tau_0 + \tau_1, \tag{5.16}$$

τ_0 is the control part that eliminates the known terms of the system and τ_1 is designed to absorb disturbances.

Now, (5.15) can be expressed as

$$\dot{e}_2 = -M^{-1}\left(Cx_2 + G\right) + M^{-1}\tau_0 + M^{-1}\tau_1 + P(t) - \dot{x}_{2ref}, \tag{5.17}$$

where

$$\tau_0 = \left(Cx_2 + G\right) + M\dot{x}_{2ref}. \tag{5.18}$$

Then $\dot{e}_2$ is expressed as

$$\dot{e}_2 = M^{-1}\tau_1 + P(t). \tag{5.19}$$

Now, the control τ_1 is proposed as [11]

$$\tau_1 \;=\; M\left(-k_2|e_2|^{\frac{1}{2}}\; sign\left(e_2\right) + \mu\right), \tag{5.20}$$

where μ is an auxiliary variable of *Super Twisting* technique.

Finally, the (5.20) is replaced in (5.19) such that

$$\begin{aligned} \dot{e}_2 &= -k_2|e_2|^{\frac{1}{2}}\; sign\left(e_2\right) + \mu + P(t), \\ \dot{\mu} &= -k_3\; sign\left(e_2\right). \end{aligned} \tag{5.21}$$

Performing the transformation $\xi = \mu + P(t)$, we obtain

$$\dot{e}_2 = -k_2|e_2|^{\frac{1}{2}}\ sign(e_2) + \xi \tag{5.22}$$
$$\dot{\xi} = -k_3\ sign(e_2) + \dot{P}(t) \tag{5.23}$$

5.2.1. Stability. The stability proof was originally done by Moreno, J. A. [11]. It is included here for sake of completeness. The perturbation of the system are globally bounded by

$$\left|\dot{P}(t)\right| \leq \delta, \tag{5.24}$$

where $\delta \geq 0$. The origin is a point of equilibrium strong, globally and asymptotically stable if the gains proposed in [11] satisfy

$$\begin{aligned} k_2 &> 0, \\ k_3 &> 3\delta + 2\frac{\delta}{k_2}^2. \end{aligned} \tag{5.25}$$

More over, all trajectories converge in finite time to the origin, bounded by $\tilde{T} = \frac{2V^{1/2}(x_0)}{\tilde{\gamma}}$, where x_0 is the inicial state and $\tilde{\gamma}$ is a constant that depend of the gains k_2, k_3 and the disturbance coefficient δ.

The Lyapunov function for the system (5.21) is expressed as

$$V = 2k_3\left|e_2\right| + \frac{1}{2}\left(k_2\left|e_2\right|^{1/2}\ sign\left(e_2\right) - \mu\right)^2. \tag{5.26}$$

The time derivative of (5.26) is

$$\dot{V} = -\frac{1}{\left|e_2\right|^{1/2}}\zeta^T Q\zeta + \frac{P(t)}{\left|e_2\right|^{1/2}}\eta_1^T\zeta, \tag{5.27}$$

where
$\eta_1^T = \begin{bmatrix} \left(2k_3 + \frac{k_2^2}{2}\right) & -\frac{k_2}{2} \end{bmatrix}, \eta_2^T = \begin{bmatrix} -k_1 & 2 \end{bmatrix}, \zeta^T = \begin{bmatrix} \left(|e_2|^{1/2}\ sign\left(e_2\right)\right) & \mu \end{bmatrix}$
and
$Q = \frac{k_2}{2}\begin{bmatrix} 2k_3 + k_2^2 & -k_2 \\ -k_2 & 1 \end{bmatrix}$.

Using the bound on the disturbance (5.24) and some algebraic manipulation, one can obtain

$$\dot{V} \leq -\frac{1}{\left|e_2\right|^{1/2}}\zeta^T\tilde{Q}\zeta, \tag{5.28}$$

where

$$\tilde{Q} = \frac{k_2}{2}\begin{bmatrix} 2k_3 + k_2^2 - 2\delta & -\left(k_2 + \frac{2\delta}{k_2}\right) \\ -\left(k_2 + \frac{2\delta}{k_2}\right) & 1 \end{bmatrix}. \tag{5.29}$$

The function (5.28) is negative definite if $\tilde{Q} > 0$, this is fulfilled under the conditions given in (5.25). In this way the state converges to zero in finite time, at most after $T = \frac{2V^{1/2}(x_0)}{\tilde{\gamma}}$ units of time, where $\tilde{\gamma} = \frac{\lambda_{min}^{1/2}\{P\}\lambda_{min}\{\tilde{Q}\}}{\lambda_{max}\{P\}}$.

With this consideration, it is obtained that $x_2 = x_{2ref}$, $e_2 = 0$ in (5.14) and $\xi = 0$ this means that $\mu = -P(t)$.

Substituting (5.13) in (5.12) is proved that

$$\dot{e}_1 = -k_1 e_1. \tag{5.30}$$

Now, the Lyapunov function for (5.30) is

$$V_1 = \frac{1}{2} e_1^T e_1, \tag{5.31}$$

that is positive definite and its time derivative is expressed as

$$\begin{aligned} \dot{V}_1 &= e_1^T \dot{e_1} = {e_1}^T \left[-k_1 e_1\right] = -{e_1}^T k_1 e_1, \\ &\leq -k_1 \left\|e_1\right\|^2. \end{aligned} \tag{5.32}$$

If the condition $k_1 > 0$ is fulfilled, (5.32) is negative definite and its origin is a equilibrium point globally and asymptotically stable.

5.3. Exact Robust Differentiator

In order to implement the control law defined in (5.9), we need to know the derivatives $\dot{y}_{ref}(t)$, $\ddot{y}_{ref}(t)$. Obviously, these are unknown terms, because only the reference vector $y_{ref}(t)$ was obtained from direct measuring from a walking person. This lacking information can be achieved by means of a robust differentiator based on high order sliding modes [9]. The structure of a 5^{th}-order differentiator is defined as follows

$$\begin{aligned} &\dot{z}_0 = v_0, \quad v_0 = -12|z_0 - y_{ref}(t)|^{5/6} sign\left(z_0 - y_{ref}(t)\right) + z_1, \\ &\dot{z}_1 = v_1, \quad v_1 = -8|z_1 - v_0|^{4/5} sign\left(z_1 - v_0\right) + z_2, \\ &\dot{z}_2 = v_2, \quad v_2 = -5|z_2 - v_1|^{3/4} sign\left(z_2 - v_1\right) + z_3, \\ &\dot{z}_3 = v_3, \quad v_3 = -3|z_3 - v_2|^{2/3} sign\left(z_3 - v_2\right) + z_4, \\ &\dot{z}_4 = v_4, \quad v_4 = -1.5|z_4 - v_3|^{1/2} sign\left(z_4 - v_3\right) + z_5, \\ &\dot{z}_5 = -1.1 sign\left(z_5 - v_4\right), \end{aligned} \tag{5.33}$$

where z_i is the estimated i^{th} derivative of y_{ref}, and whose initial value is zero.

Figure 3 shows the bio-inspired walking references for the six joints of the left leg and the output of the robust differentiator for the first and second derivatives.

The Figure 4 shows all the bio-inspired signals for each joint of the legs.

6. Simulations

The proposed control law defined in (5.9) was applied to the biped robot shown in Figure 2. The axes of rotation are proposed in Figure 6. The initial value of vector for the both legs is $x_0 = 10^{-2} \cdot \begin{bmatrix} 5 & 21 & 8 & 62 & 15 & 0.003 \end{bmatrix}^T$, the gains k_1, k_2 were set as $k_1 = 10 \cdot \begin{bmatrix} 1 & 4 & 1 & 4 & 4 & 2 \end{bmatrix}^T$ and $k_2 =$

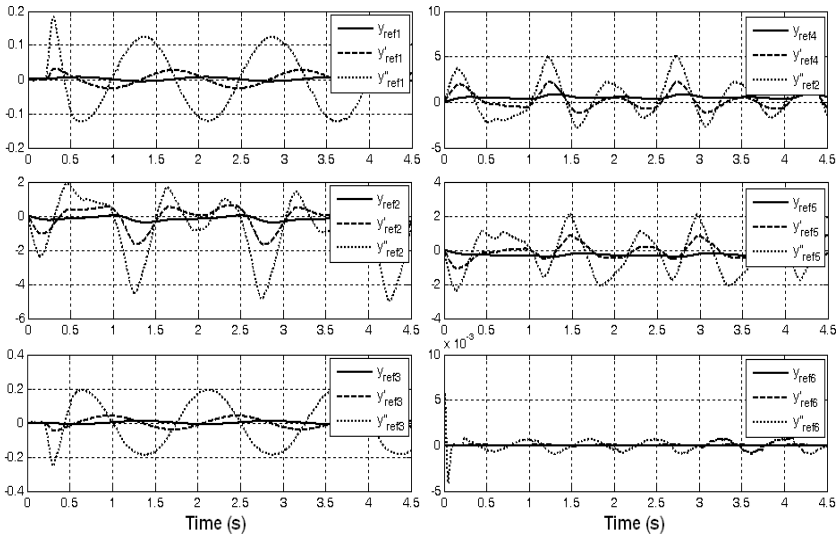

FIGURE 3. Reference signal, first derivative, and second derivative for the six joints of left leg.

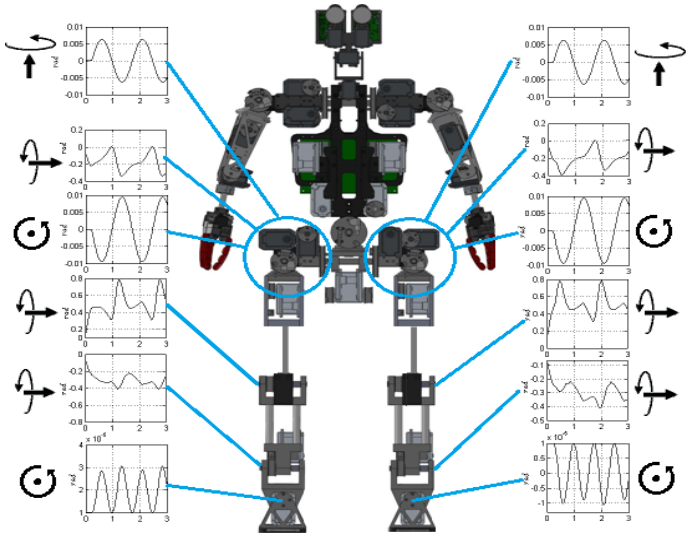

FIGURE 4. Bio-inspired reference signal for the joints of each leg.

$10 \cdot \begin{bmatrix} 1 & 28 & 1 & 28 & 14 & 4 \end{bmatrix}^T$, respectively. The slopes ε_1, ε_2 were chosen as $\varepsilon_1 = 2$, $\varepsilon_2 = 5$.

The initial position for the center of mass of each link are

$$\begin{aligned} x_1 &= \sigma_1 e_1 - \sigma_2 e_2, & x_7 &= -\sigma_1 e_1 - \sigma_2 e_2, \\ x_2 &= \sigma_3 e_1 - \sigma_2 e_2, & x_8 &= -\sigma_3 e_1 - \sigma_2 e_2, \\ x_3 &= \sigma_4 e_1 - \sigma_5 e_2, & x_9 &= -\sigma_4 e_1 - \sigma_5 e_2, \\ x_4 &= \sigma_4 e_1 - \sigma_6 e_2, & x_{10} &= -\sigma_4 e_1 - \sigma_6 e_2, \\ x_5 &= \sigma_4 e_1 - \sigma_7 e_2, & x_{11} &= -\sigma_4 e_1 - \sigma_7 e_2, \\ x_6 &= \sigma_4 e_1 - \sigma_8 e_2, & x_{12} &= -\sigma_4 e_1 - \sigma_8 e_2, \end{aligned} \tag{6.1}$$

and the origins of the frames attached to each link of the biped robot are the following Euclidean points, these points can be expressed in conformal geometric algebra to equation (2.1).

$$\begin{aligned} o_1 &= \sigma_9 e_1 - \sigma_2 e_2, & o_7 &= -\sigma_9 e_1 - \sigma_2 e_2, \\ o_2 &= \sigma_4 e_1 - \sigma_2 e_2, & o_8 &= -\sigma_4 e_1 - \sigma_2 e_2, \\ o_3 &= \sigma_4 e_1 - \sigma_3 e_2, & o_9 &= -\sigma_4 e_1 - \sigma_3 e_2, \\ o_4 &= \sigma_4 e_1 - \sigma_{10} e_2, & o_{10} &= -\sigma_4 e_1 - \sigma_{10} e_2, \\ o_5 &= \sigma_4 e_1 - \sigma_8 e_2 = o_6, & o_{11} &= -\sigma_4 e_1 - \sigma_8 e_2 = o_{12}, \end{aligned} \tag{6.2}$$

with $\sigma_1 = 0.024$, $\sigma_2 = 0.062$, $\sigma_3 = 0.079$,$\sigma_4 = 0.110$, $\sigma_5 = 0.068$, $\sigma_6 = 0.188$, $\sigma_7 = 0.417$, $\sigma_8 = 0.533$, $\sigma_9 = 0.049$ and $\sigma_{10} = 0.302$ which all depend on the magnitude of the distances between the reference frame $\{e_1, e_2, e_3\}$ and the origins o_i, $i = 1, ..., 12$ indicated in Figure 5.

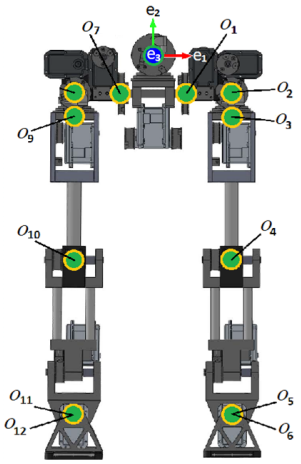

FIGURE 5. Origins of the frames attached to each link.

The initial values for the axes of rotation of the biped robot are defined as

$$
\begin{aligned}
L_1 &= e_{23} + e_\infty (o_1 \cdot e_{23}), & L_7 &= e_{23} + e_\infty (o_7 \cdot e_{23}), \\
L_2 &= e_{12} + e_\infty (o_2 \cdot e_{12}), & L_8 &= e_{12} + e_\infty (o_8 \cdot e_{12}), \\
L_3 &= e_{31} + e_\infty (o_3 \cdot e_{31}), & L_9 &= e_{31} + e_\infty (o_9 \cdot e_{31}), \\
L_4 &= e_{23} + e_\infty (o_4 \cdot e_{23}), & L_{10} &= e_{23} + e_\infty (o_{10} \cdot e_{23}), \\
L_5 &= e_{23} + e_\infty (o_5 \cdot e_{23}), & L_{11} &= e_{23} + e_\infty (o_{11} \cdot e_{23}), \\
L_6 &= e_{12} + e_\infty (o_6 \cdot e_{12}), & L_{12} &= e_{12} + e_\infty (o_{12} \cdot e_{12}).
\end{aligned}
\tag{6.3}
$$

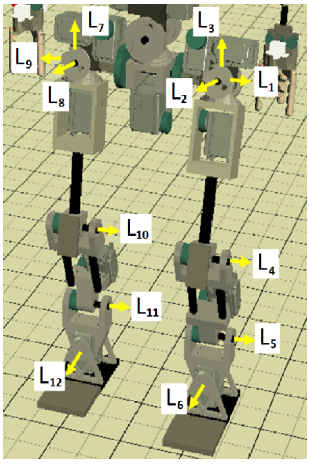

FIGURE 6. Axes of rotation of the biped robot.

The simulation results for the left leg are next shown. The performance and response for the right leg are very similar to the left leg and are not included. The disturbance signals used in simulation can be appreciated in Figure 7.

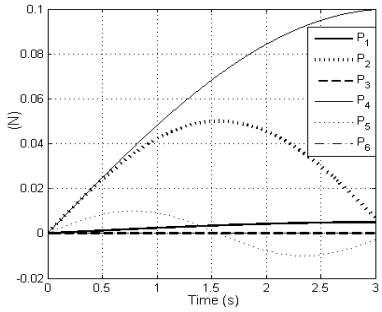

FIGURE 7. Disturbances used in simulation for each joint of left leg.

6.1. Simulations using first order sliding mode control

The tracking responses for the six joints of the left leg are depicted in Figure 8. It can be observed that the control objective is fulfilled and with a low settling time.

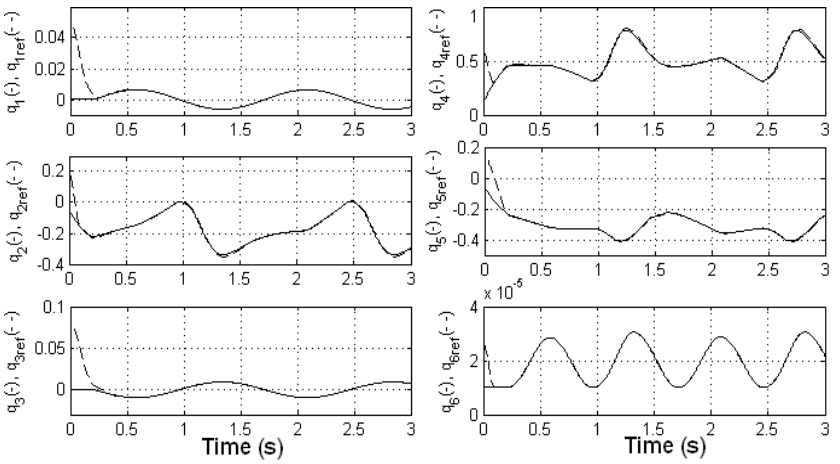

FIGURE 8. Tracking response for the 6 joints of the left leg (1^{st} order sliding mode control).

Figure 9 shows that the six corresponding error variables converge to a small vicinity of zero, demonstrating the robustness of the proposed control scheme.

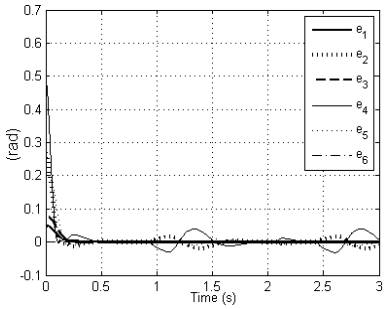

FIGURE 9. Tracking error for the 6 joints of the left leg (1^{st} order sliding mode control).

In Figure 10, the control signals (joint torques) of the left leg are depicted.

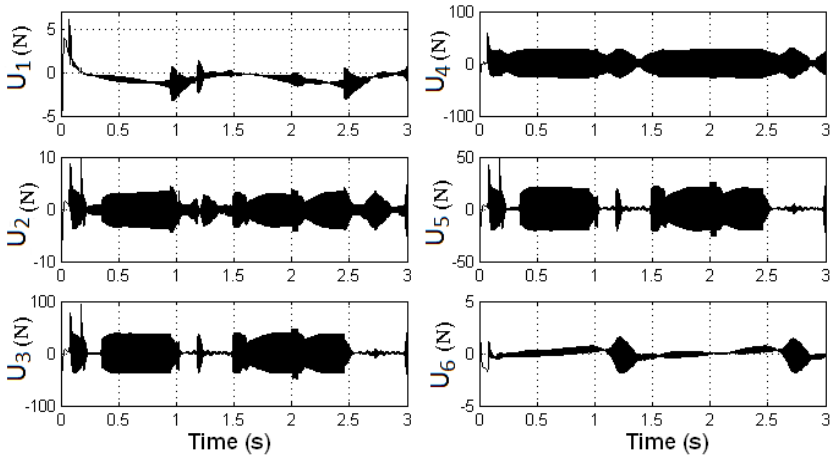

FIGURE 10. Control signals (joint torques) for the six joints of the left leg (1^{st} order sliding mode control).

6.2. Simulations using super twisting technique

The tracking responses for the 6 joints of the left leg are depicted in Figure 11. It can be observed that the control objective is fulfilled and with a low settling time.

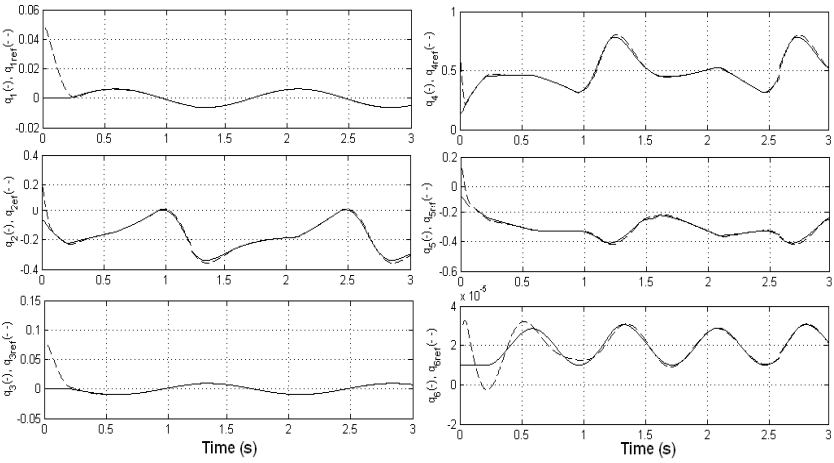

FIGURE 11. Tracking response for the 6 joints of the left leg (*super twisting* technique).

Figure 12 shows that the six corresponding error variables converge to a small vicinity of zero using *super twisting* technique, demonstrating the robustness of the proposed control scheme.

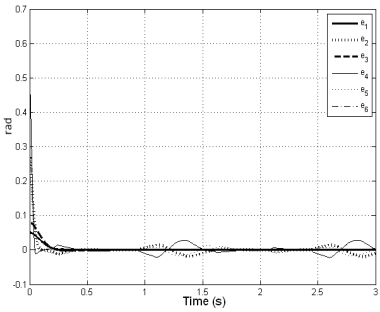

FIGURE 12. Tracking error for the 6 joints of the left leg (*super twisting* technique).

In Figure 13, the control signals (joints torques) of the left leg are depicted, using *super twisting* technique. The high frequency components is significantly attenuated unlike the Figure 10 even though the setting time is a bit longer than the control schema using first order sliding mode control.

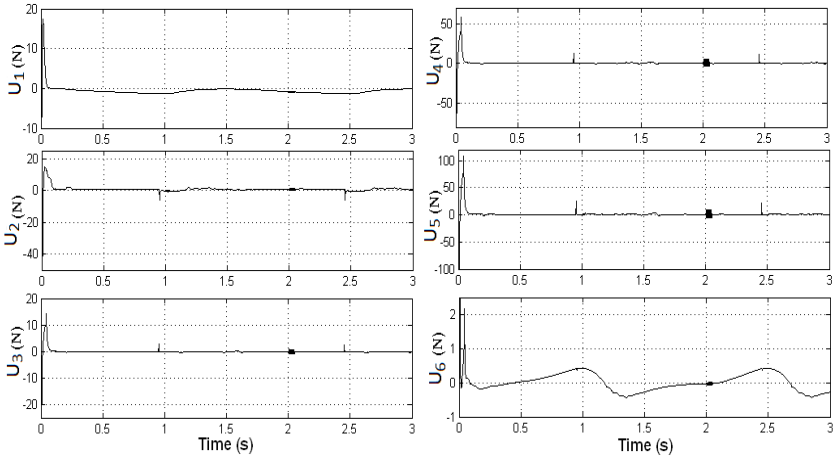

FIGURE 13. Control signals (joint torques) for the six joints of the left leg (*super twisting* technique).

Finally, a sequence of images of the biped robot walking is presented in Figure 14.

7. Conclusions

The authors apply bio-inspired signals as walking waves as references for the walking of a humanoid robot. The advantage of using such signal is that they help us to accomplish an expected human like walking of the robot. However

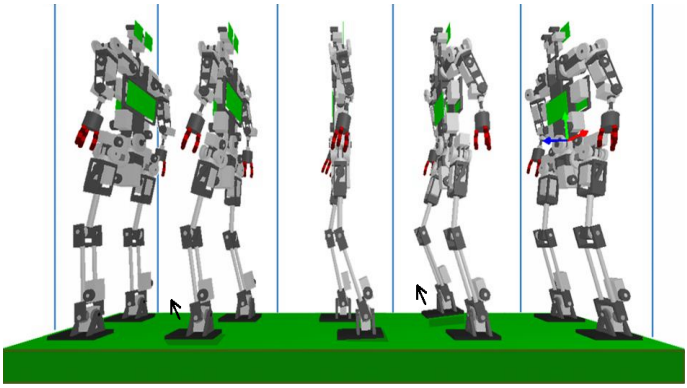

FIGURE 14. Sequence of images of the biped robot walking (two steps).

this is jeopardized due to the effect of perturbations and non-modelled parameters of the robot dynamics. To follow such trajectories is necessary to resort to a robust control techniques. In addition the algebraic complexity of the formulation is also an issue, which is tackled by computing the kinematics and dynamics of the plant in the conformal geometric algebra framework. As a result, the equations are simple, compact and comfortable to design algorithms subject to geometric constraints. In this regard, the use of a robust sliding mode controllers becomes easy and natural. We present simulations subject to perturbations which confirm the robustness of our control schemes. Future work consists of using more advanced control techniques and real time implementation.

References

[1] Bayro-Corrochano Eduardo, *Geometric Computing: for Wavelet Transforms, Robot Vision, Learning, Control and Action*. Springer Verlag, London, Jan, 2010.

[2] http://www.pupin.rs/RnDProfile/robotics/hrsp.html

[3] http://www.pupin.rs/RnDProfile/rodic-pub.html

[4] V. I. Utkin, J. Guldner and J. Shi *Sliding Mode Control in Electromechanical Systems*. Taylor and Francis, 1999.

[5] H. Li , D. Hestenes, and A. Rockwood, *Generalized Homogeneous coordinates for computational geometry*. In G. Somer, editor, "Geometric Computing with Clifford Algebras", pp. 27-52. Springer-Verlag Heidelberg, 2001.

[6] J. Zamora and E. Bayro-Corrochano, "Kinematics and Differential Kinematics of Binocular Heads". *Proceedings of the International Conference of Robotics and Automation (ICRA'06)*, Orlando, Florida, USA, 2006, pp. 4130-4135.

[7] J. Zamora and E. Bayro-Corrochano, "Parallel Forward Dynamics: a geometric approach", *Proceedings of the International Conference on Intelligent Robots and Systems, IROS 2010*, Taiwan, pp. 18-22, 2010.

[8] L. Gonzáles-Jiménez, A. Loukianov and E. Bayro-Corrochano *Integral Nested Sliding Mode Control for Robotic Manipulators.* Proceedings of the 17th World Congress The International Federation of Automatic Control, Seoul, Korea, 2008, pp. 9899 – 9904.

[9] A. Levant, "Higher Order Modes, Differentiation and Output Feedback Control, *International Journal of Control* , Vol. 76, pp. 924 - 941, 2003.

[10] A. Levant, "Sliging order and sliding accuracy in sliding mode control, *International Journal of Control* , Vol. 58, 1247 - 1263, 1993.

[11] J. A. Moreno, M. Osorio, "A Lyapunov approach to second-order sliding mode controllers and observers, In *Proc. of the 47th Conf. on Decision and Control.* Cancún, México, pages 2856-2861, December 9-11, 2008.

[12] J. Oviedo-Barriga, O. Carbajal-Espinosa, L. Gonzlez-Jimnez, Bernardino Castillo-Toledo, Eduardo Jose Bayro-Corrochano. "Robust Tracking of Bio-Inspired References for a Biped Robot Using Geometric Algebra and Sliding Mode, in *IEEE International Conference on Robotics and Automation*, Karlsruhe, Germany, 2013

J. Oviedo-Barriga
Av. Del Bosque 1145, Col. El Bajío,
C.P. 45019, Zapopan, Jalisco, México
e-mail: joviedo@gdl.cinvestav.mx

L. González-Jiménez
Av. Del Bosque 1145, Col. El Bajío,
C.P. 45019, Zapopan, Jalisco, México
e-mail: lgonzale@gdl.cinvestav.mx

B. Castillo-Toledo
Av. Del Bosque 1145, Col. El Bajío,
C.P. 45019, Zapopan, Jalisco, México
e-mail: toledo@gdl.cinvestav.mx

E. Bayro-Corrochano
Av. Del Bosque 1145, Col. El Bajío,
C.P. 45019, Zapopan, Jalisco, México
e-mail: edb@gdl.cinvestav.mx